Geophys. J. Int. (1992) **110**, 451–464

Particle motion and the modelling of strain response in magnetic fabrics

Carl Richter
Department of Geological Sciences, University of Michigan, Ann Arbor, MI 48109, USA

Accepted 1992 March 18. Received 1992 January 23; in original form 1991 July 18

SUMMARY

Quantitative correlations between the magnetic fabric (magnetic susceptibility or remanent magnetic anisotropies), single mineral anisotropy, and preferred mineral orientation is investigated using computer modelling. The influences of various initial fabric patterns and imposed strain on the magnetic fabric are simulated using multiparticle systems represented by their magnetic anisotropy tensor. Each single mineral is numerically reoriented under coaxial deformation conditions using the strain response models of March and Jeffery/Gay. The calculated strain $\ln(e_i)$ versus magnetic fabric $M_i = \ln[k_i/(k_{max} \cdot k_{int} \cdot k_{min})^{1/3}]$ curves show the following characteristics: (1) for initial randomly oriented distributions a log–linear correlation exists for strain magnitudes below 200 per cent. (2) For higher strains the curves asymptotically approach the M_i value defined by the particle anisotropy. (3) The slope α of the correlation lines is a function of the particle anisotropy, the ellipsoid shape, and the strain response model. (4) Due to the prolate shape of particles, the maximum susceptibility axes are more sensitive to strain for initially anisotropic fabrics than the minimum axes. (5) The relationship between magnetic fabric and strain in multiparticle systems with known initial preferred orientations and single particle anisotropy shows a similar behaviour. Depending on the pattern and orientation of the initial fabric, the maximum axes show either a log–linear correlation to strain with a characteristic slope α or a kinked curve, with two almost linear parts.

Key words: anisotropy of magnetic susceptibility, Jeffery/Gay model, magnetic fabrics, March model, preferred mineral orientation, strain analysis.

INTRODUCTION

Efforts have been made in numerous studies to use magnetic fabrics (mainly the anisotropy of magnetic susceptibility, AMS, and to minor extent remanent anisotropies) as an indicator of the direction and magnitude of strain (e.g. Rathore 1980; Henry & Daly 1983; review by Borradaile 1991). All of these investigations demonstrated a parallelism between the principal AMS axes orientations and the major petrofabric features. Some studies proposed an empirical quantitative correlation between parameters of the magnitudes of strain and the corresponding magnitudes of AMS (e.g. Rathore 1980; Hirt 1986; Ruf *et al.* 1988; Cogné & Perroud 1988). A quantitative correlation between the two tensors is expected only in rocks of identical initial fabric and homogeneous mineral composition. This, however, is never strictly fulfilled in natural rocks and is difficult to simulate by experimental procedures (e.g. Borradaile & Puumala 1989; Richter *et al.* 1992). Hence, numerical methods currently provide the best tool to gain information on the pathway that is followed by magnetic fabrics during increasing strain, and to investigate the influences of mineralogical composition, strain geometry, and initial fabric on the magnitudes of magnetic fabrics (e.g. Richter 1991).

Applications and problems of the measurement of magnetic fabrics were reviewed by Hrouda (1982) and more recently by Borradaile (1988, 1991). Quantitative correlations between AMS and strain have widely been criticized because of the strong dependence of the susceptibility magnitudes on the mineral composition (Borradaile 1987; Borradaile *et al.* 1987). AMS commonly reflects variations in mineral composition rather than strain. Techniques such as the measurement of remanent anisotropies (McCabe, Jackson & Ellwood 1985), hysteresis loops, and cold temperature experiments (Schultz-Krutisch & Heller 1985)

can, however, be used to measure parts of the AMS tensor separately, or to demonstrate the dominance of one component (significant mineral). Magnetic fabrics which are dominated by a single mineral measure the crystallographic preferred orientation of the paramagnetic and most ferrimagnetic minerals, or the preferred orientation of grain axes of magnetic (Uyeda *et al.* 1963).

The anisotropy of magnetic susceptibility is used in this paper as an example of an anisotropic magnetic property (the term 'magnetic fabric' includes all types of anisotropies). I emphasize that the modelling does not support the idea of an AMS–strain correlation in general. A simple correlation between strain and AMS magnitudes may exist in certain cases, but varying mineral compositions are likely to overprint strain induced anisotropies (Borradaile 1987). Strain correlations are much more likely for components of the AMS tensor, or for a one-mineral dominated AMS. Anisotropic magnetic properties, such as the anisotropy of anhysteretic susceptibility (AAS, McCabe *et al.* 1985), the anisotropy of isothermal remanent magnetization, or the anisotropy of thermoremanent magnetization (e.g. Cogné 1987) may also produce valid strain correlations.

The AMS is the tensor that relates the intensity of the applied external field (H) to the acquired magnetization (M) of a material:

$$M_i = \boldsymbol{k}_{ij} H_j, \tag{1}$$

with the proportionality factor $\boldsymbol{k}_{ij}$ being a second rank tensor referred to as the susceptibility tensor (e.g. Hrouda 1982; Nye 1985). The susceptibility tensor is expressed by its principal susceptibility magnitudes $k_{max} \geq k_{int} \geq k_{min}$ (or $k_{11} \geq k_{22} \geq k_{33}$) and their orientations. The degree of anisotropy $P = k_{max}/k_{min}$ (Nagata 1961) is used to describe the shape of the susceptibility ellipsoid. The magnitudes are denoted as volume susceptibility in SI units (their absolute values are of minor importance in this context). The strain magnitude is expressed as the elongation e. It is the ratio between the relative change of length of a line (Δl) and the initial length (l) of the line $e = \Delta l/l$. The natural strain or logarithmic strain ϵ is defined as the natural logarithm of the principal strain magnitudes $\epsilon = \ln(l + e)$ and the strain magnitude in per cent is $100e$ per cent.

The AMS of a crystal aggregate is the resultant of the anisotropy effects of all phases and particles and, therefore, a function of the mineral composition (Borradaile *et al.* 1987), the grain shape (Uyeda *et al.* 1963), and the preferred mineral orientation. A rock sample in an orthogonal reference frame ($0x$, $0y$, $0z$) has a total anisotropy that is defined by its susceptibility tensor $(\boldsymbol{k}_{ij})_j$. One single particle (mineral or grain) of a rock is represented by

$$(\boldsymbol{k}_{ij})_p = \begin{pmatrix} k_{11} & k_{12} & k_{13} \\ k_{21} & k_{22} & k_{23} \\ k_{31} & k_{32} & k_{33} \end{pmatrix}. \tag{2}$$

For a monomineralic crystal aggregate or a one-mineral dominated AMS the total susceptibility $(\boldsymbol{k}_{ij})_t$ is calculated by the summation of the particle tensors using

$$(\boldsymbol{k}_{ij})_t = \sum (\boldsymbol{k}_{ij})_p, \tag{3}$$

and neglecting any physical interactions between the single grains. Also, anisotropy effects resulting from a non-isotropic distribution of grains, for example in layers, are not taken into consideration.

In the models presented in this paper, single particles represented by their anisotropy tensor are individually reoriented using models of strain response proposed by March (1932) and Gay (1968), based on the work of Jeffrey (1923). Both of these models require passive rotation of the significant susceptibility carriers and do not account for processes occurring in natural rocks like recrystallization, pressure solution, or grain interference. However, they are well-established strain response models that are applicable in specific circumstances (Oertel 1983), but certainly not in every case. With these limitations in mind I think the model calculations can be used (i) to show principal relationships between magnetic anisotropies and strain, (ii) to demonstrate the effects of initial fabric, grain shape, and single particle anisotropy on quantitative correlations, and (iii) to determine finite strain magnitudes from magnetic fabric data if the assumptions of the model are fulfilled.

The model offers the possibility to simulate the deformation of a rock with an initial distribution of mineral axes and consisting of rigid particles with different magnetic properties. The initial grain distribution was achieved by a random function of the computer. To produce initial fabrics with gridle or point distribution patterns, the strike or dip was limited to selected values. The fabric development is shown in lower hemisphere, equal area sterographic projections of the produced grain distribution, i.e. the tensor orientations.

A DYNAMIC APPROACH: THE STRAIN RESPONSE OF MAGNETIC FABRICS

The effect of strain on AMS is simulated by considering single grains that are represented by their susceptibility tensor $(\boldsymbol{k}_{ij})_p$. The principal directions of $(\boldsymbol{k}_{ij})_p$ are determined by grain shape (magnetite) or by the crystallographic lattice. For simplicity, the following considerations are restricted to prolate ellipsoids of revolution. The orientation of a single grain, hence, is determined by the polar coordinates θ and ϕ of its symmetry axis. For a prolate grain with the principal susceptibilities $k_a \geq k_b = k_c$ the complete susceptibility tensor with respect to the reference frame is written

$$(\boldsymbol{k}_{ij})_p = \begin{pmatrix} k_{11} & k_{12} & k_{13} \\ k_{21} & k_{22} & k_{23} \\ k_{31} & k_{32} & k_{33} \end{pmatrix}, \tag{4}$$

where for a prolate grain, since $(\boldsymbol{k}_{ij})_p$ is a symmetrical tensor (Owens 1974; Hrouda *et al.* 1985);

$$\begin{aligned} k_{11} &= (k_a - k_b)\sin^2\theta\cos^2\phi + k_b \\ k_{22} &= (k_a - k_b)\sin^2\theta\sin^2\phi + k_b \\ k_{33} &= (k_a - k_b)\cos^2\theta + k_b \\ k_{12} &= k_{21} = (k_a - k_b)\sin^2\theta\sin\phi\cos\phi \\ k_{23} &= k_{32} = (k_a - k_b)\sin\theta\cos\theta\sin\phi \\ k_{13} &= k_{31} = (k_a - k_b)\sin\theta\cos\theta\cos\phi. \end{aligned} \tag{5}$$

This set of equations is used to calculate $(\boldsymbol{k}_{ij})_p$ for a grain with the orientation θ, ϕ. The total AMS of a polycrystal is

obtained by summing up the individual tensors. In the following model calculations, a set of 200–300 grains was used. The initial orientation θ, ϕ for each grain was produced using the random function of the computer. After calculation of the individual grain susceptibility $(\boldsymbol{k}_{ij})_p$ and summation of the tensors, the initial magnetic fabric was obtained by the calculation of the eigensystem of the total tensor. This yields the orientation and the principal magnitudes of the resulting magnetic fabric. The flowchart in Fig. 1 shows the schematic procedure of the calculations.

Strain has the effect of modifying the orientation θ, ϕ of each particle into a new direction θ', ϕ'. The mathematical formulation of the motion of individual particles during strain, the strain response model, is the critical problem when simulating the behaviour of magnetic fabrics during strain. Though advances have been made in the formulation of strain response (Jeffrey 1923; March 1932; Bhattacharyya 1966; Gay 1966, 1968; Owens 1973, 1974; Reed & Tryggvason 1974; Ramberg 1975; Hrouda 1980), a realistic approach is difficult to obtain.

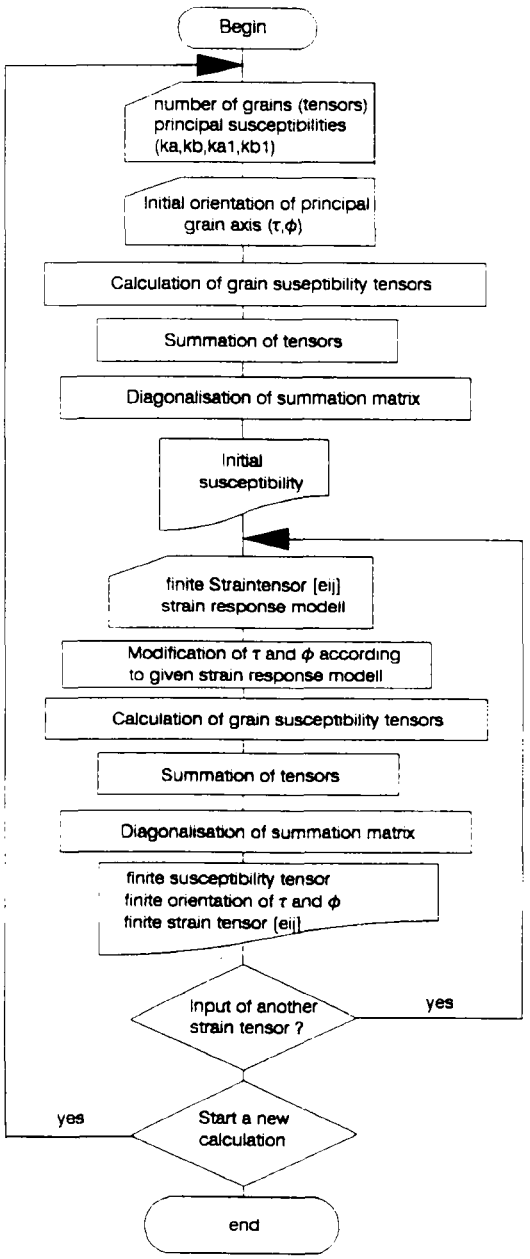

Figure 1. Generalized flow chart of the calculation of the resulting magnetic fabric before and after the modification of the individual grain orientation by a given strain tensor $(\boldsymbol{e}_{ij})$.

The approach of Artur March (1932) has been commonly applied for a quantitative interpretation of phyllosilicate fabrics (e.g. Oertel 1983). More sophisticated models that take the ductility contrast between the matrix and minerals into account were first proposed by Einstein (1896) for spherical particles and extended to the case of ellipsoidal particles by Jeffrey (1923). The general equations of Jeffrey were modified by Gay (1966, 1968a), who considered the case of an ellipsoid of revolution in a pure shear field.

After the selection of a strain response model and the magnitudes and geometry of strain, the determination of θ', ϕ' for each individual grain is carried out by calculating the new single mineral tensors. Summation of the $(\boldsymbol{k}_{ij})_g$ yields the total magnetic fabric. The eigensystem of the total tensor provides orientation and magnitude data from the strain magnetic fabric. I wrote a computer program to simulate the strain response of magnetic fabrics for individual grains using different strain response models (see flowchart Fig. 1). The development of multiparticle systems is shown in lower hemisphere equal area projections of the xy-plane, with z vertically and x oriented to the north. The particle motion is thus visualized and can be compared with strain and the magnitudes of the magnetic fabric. The axes x, y, z of the coordinate system were selected so that e_{11} is parallel to x, e_{22} parallel to y, and e_{33} parallel to z.

The March model

March's model (March 1932) of the rearrangement of thin tabular or rod-shaped grains in a strained rock is not concerned with the behaviour of real crystal grains in a rock matrix with different properties, but with the geometrical consequences of homogeneous strain affecting all components of the material uniformly. Grains are assumed to be mechanically indistinguishable from the rock matrix in which they are embedded and only play the role of markers.

Homogeneous deformation in an orthogonal reference frame is described by a linear equation set, that characterizes the translation of a material point (x, y, z) prior to deformation to the point (x', y', z') after the deformation (e.g. Means 1976):

$$\begin{aligned} x &= e_{11}x' + e_{12}y' + e_{13}z', \\ y &= e_{21}x' + e_{22}y' + e_{23}z', \\ z &= e_{31}x' + e_{32}y' + e_{33}z'. \end{aligned} \tag{6}$$

Considering a line (the normal of a tabular grain or the long axis of a rod-shaped grain) in a Cartesian coordinate system with the usual polar coordinates (θ, ϕ), the strained line has the coordinates (θ', ϕ'). Using trigonometrical relations between polar and Cartesian coordinates (e.g. Bronstein & Semendjaev 1987) the above equations are

modified to (March 1932):

$$\begin{aligned} r^* \sin\theta\cos\phi &= r'[\sin\theta'(e_{11}\cos\phi' + e_{12}\sin\phi') + e_{13}\cos\theta'], \\ r^* \sin\theta\sin\phi &= r'(\sin\theta'(e_{21}\cos\phi' + e_{22}\sin\phi') + e_{23}\cos\theta'], \\ r^* \cos\phi &= r'[\sin\theta'(e_{31}\cos\phi' + e_{32}\sin\theta') + e_{33}\cos\theta'], \end{aligned} \tag{7}$$

where r is the length of the line before deformation and r' the length of the deformed line. Introducing the quadratic elongation $\lambda = (r'/r)^2$, the equations transform to

$$\begin{aligned} \sin\theta\cos\phi &= [\sin\theta'(e_{11}\cos\phi' + e_{12}\sin\phi') + e_{13}\cos\theta']/\lambda = A_1/\lambda, \\ \sin\theta\sin\phi &= [\sin\theta'(e_{21}\cos\phi' + e_{22}\sin\phi') + e_{23}\cos\theta'/\lambda = A_2/\lambda, \\ \cos\phi &= [\sin\theta'(e_{31}\cos\phi' + e_{32}\sin\phi') + e_{33}\cos\theta'/\lambda = A_3/\lambda. \end{aligned} \tag{8}$$

These equations are solved to find the relation between (θ, ϕ) and (θ', ϕ') for any given e_{ij}:

$$\theta' = \arctan\{\mathrm{sqrt}[(A_1)^2 + (A_2)^2]/A_3\},$$

$$\phi' = \arctan(A_2/A_1).$$

Results from the March model

I first describe the influences of coaxial plane strain on an initially isotropic distribution ($P = 1.01$) of 300 particles (Fig. 2). Each point represents the polar coordinates θ, ϕ of the maximum susceptibility axes. Since $k_{int} = k_{min}$ this suffices to describe the orientation of the total tensor in the reference frame. The assumed degree of anisotropy of the single grains is $P = 1.75$ and is on the order of measured single mineral values (e.g. Borradaile *et al.* 1987). Fig. 2 illustrates the change in the distribution pattern for various strain magnitudes. Table 1 gives the magnitudes of strain and the calculated principal susceptibilities.

The observed particle path reflects the establishment of perferred orientation with increasing deformation. The semi-major axes rotate away from the compressional axis towards the stretching direction. For a given deformation increment, grains with steep dips have a small rotation angle compared to the grains with an intermediate dip.

Fig. 3(a) traces the magnetic fabric path in a Flinn-type (Flinn 1962) diagram. The initial isotropic geometry is overprinted during the first deformation step and continuously evolves to increasingly prolate forms.

One method to investigate the relationship between magnetic fabric and strain is to plot the natural strain ϵ_i versus the corresponding magnetic parameter M_i (Fig. 3a), where

$$M_i = \ln[k_i/(k_1 \cdot k_2 \cdot k_3)^{1/3}]. \tag{10}$$

The maximum susceptibility axes are correlated to the maximum strain axes in the upper right quadrant of Fig. 3(b) and the minimum axes are independently correlated in the lower left quadrant. The intermediate axes are omitted. Both show a log–linear correlation with a characteristic slope α for strain magnitudes up to 200 per cent. The minimum axes, however, deflect already at 80 per cent strain from the linear path. This behaviour is caused by the magnetic properties of the considered prolate particles, for which the M_{min} cannot exceed a value of -0.187, whereas the M_{max} can reach values up to 0.373. The slope α of the correlation lines is a function of the degree of anisotropy (k_{max}/k_{min}) of the single particles. The inset of Fig. 3(b) demonstrates that the slope systematically increases with a decreasing degree of anisotropy.

The correlation between the two magnitudes as it was found in natural examples (e.g. Hirt 1986; Ruf *et al.* 1988) is thus confirmed numerically. It is valid for the case of a monomineralic polycrystal with uniformly distributed particles that deforms under conditions obeying the March model.

Influences of the imposed initial fabric were investigated with the deformation of two synthetic fabrics with a preferred orientation of 300 grains. The first one is a preferred orientation of grains inside a 45° cone around the z-axis, referred to as a z-point distribution (Cheeney 1983), and the second is a girdle distribution in the xy-plane. The initial fabric and three stages of deformation under coaxial plane strain are shown in Fig. 4. The strain magnitudes and the calculated susceptibility values are given in Table 1.

The initial magnetic anisotropy of the point distribution is strongly prolate (Fig. 5a) reaching nearly the single particle anisotropy. The initial preferred orientation is parallel to the compressional axis and during strain the points move into parallelism with the stretching direction. The prolate fabric thus first decreases (Fig. 5a) and when the points attain a girdle pattern, the magnetic fabric becomes oblate. The points, however, rotate during higher strains into parallelism with the stretching direction and finally reach a total geometry that is quite similar to the initial fabric but with a 90° rotated orientation. The geometry of the magnetic fabric during increasing coaxial deformation thus moves along a nearly straight line between a perfect prolate shape and a perfect oblate shape (shown in Flinn diagram). The quantitative correlation between strain and magnetic fabric (Fig. 5b) is strongly influenced by this phenomenon. The magnetic parameter M_i of the initial fabric ($\epsilon_i = 0$) is high, becomes successively lower until the fabric is oblate and increases again, when the particles commence to cluster around the stretching direction. A log–linear or nearly linear correlation is revealed for the increasing and decreasing branches of the maximum values. Magnetic parameters are ambiguous and can be caused by different strain magnitudes. Minimum axes rotate nearly parallel to the y-axis and hardly change their orientation. Hence, minimum susceptibilities show no correlation to strain.

The magnetic fabric development of the strained xy-girdle distribution is shown in Fig. 6(a). The initial oblate fabric evolves to a prolate geometry at a strain of 120 per cent. The maximum $\epsilon_i - M_i$ values show a log–linear correlation (Fig. 6b) for strains under 300 per cent. The correlation line, however, does not pass through the origin. The minimum values are linearly correlated up to 60 per cent strain. If this value is exceeded the M_{min} value is close to its maximum and cannot further increase because the minimum axes of most minerals are oriented in the yz-plane and the total k_{33} (compare Table 1) only slightly changes its magnitude. The k_{11} axes, on the other hand, still scatter in the xy-plane and get more aligned with increasing strain.

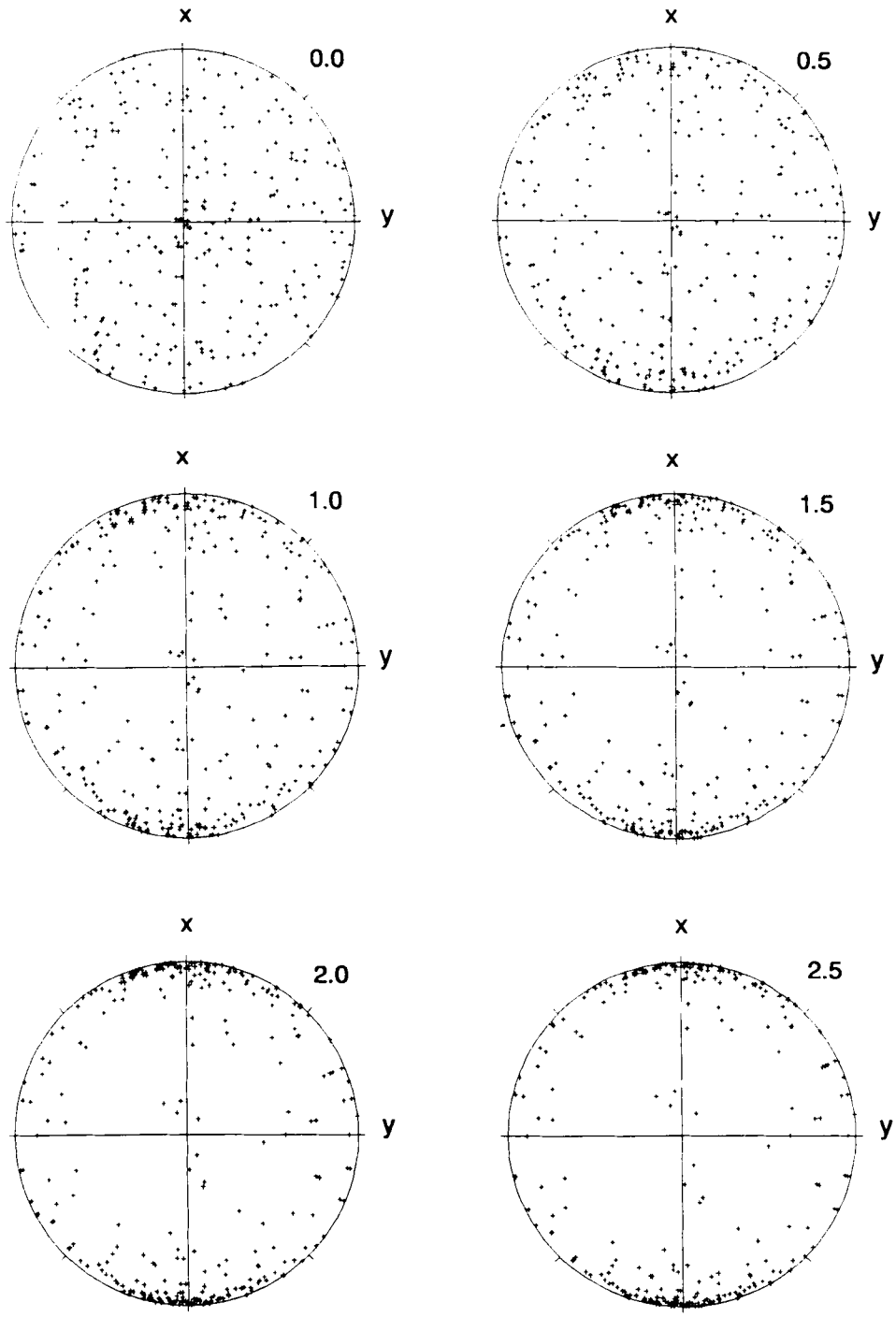

Figure 2. Fabric diagrams for 300 initial randomly distributed particles deformed under coaxial plane strain with the March model. The shortening direction is vertical and the extension direction along the x-axis. The numbers are the magnitudes of the elongation e_{11}; lower hemisphere equal area projections.

The effects of uniaxial flattening and uniaxial construction (equal volume deformations) on the initial random fabric are investigated in Fig. 7. Both strain geometries show almost the same characteristics as the plane strain deformations with an essentially identical slope of the correlation lines (compare Fig. 3b). The AMS ellipsoid shape for the oblate strain geometry is strongly oblate in all cases, and prolate for the prolate strain geometry (Table 2).

The viscous fluid (Jeffrey/Gay) model

The mathematical formulation of the motion of rigid, ellipsoidal particles embedded in a viscous fluid matrix during coaxial deformation was derived by Gay (1968a). Gay uses the general equations of Jeffrey (1923) to formulate the strain response of ellipsoids of revolution with length of the semi-major axis termed a and the length of the

Table 1. Principal strain magnitudes and susceptibilities for initial isotropic, point, and xy-girdle distributions deformed after the March model under coaxial plane strain ($e_{22} = 0$) conditions.

strain		March model: random			point			xy-girdle		
e11	e33	k11	k22	k33	k11	k22	k33	k11	k22	k33
0.0	0.00	5.03	5.00	4.98	6.46	4.28	4.26	5.24	5.11	4.65
0.1	-0.09	5.11	4.99	4.90	6.35	4.34	4.31	5.29	5.17	4.54
0.2	-0.17	5.20	4.97	4.82	6.23	4.44	4.34	5.37	5.18	4.45
0.3	-0.23	5.28	4.96	4.75	6.11	4.52	4.36	5.46	5.16	4.37
0.4	-0.29	5.37	4.94	4.69	6.00	4.62	4.39	5.55	5.14	4.31
0.5	-0.33	5.44	4.92	4.64	5.90	4.70	4.40	5.62	5.12	4.27
0.6	-0.37	5.50	4.91	4.59	5.78	4.80	4.42	5.68	5.09	4.22
0.7	-0.41	5.57	4.89	4.55	5.68	4.89	4.43	5.75	5.06	4.19
0.8	-0.44	5.62	4.87	4.51	5.59	4.97	4.44	5.80	5.04	4.17
0.9	-0.47	5.68	4.85	4.48	5.50	5.05	4.44	5.85	5.01	4.14
1.0	-0.50	5.72	4.83	4.45	5.26	5.22	4.52	5.91	5.01	4.08
1.2	-0.54	5.81	4.80	4.39	5.28	5.27	4.45	5.97	4.93	4.10
1.4	-0.58	5.89	4.76	4.35	5.39	5.15	4.46	6.04	4.89	4.07
1.6	-0.62	5.95	4.73	4.32	5.51	5.04	4.45	6.10	4.84	4.06
1.8	-0.64	6.01	4.70	4.29	5.60	4.95	4.45	6.15	4.80	4.05
2.0	-0.67	6.07	4.67	4.26	5.69	4.86	4.44	6.20	4.76	4.04
2.5	-0.71	6.17	4.61	4.22	5.88	4.70	4.42	6.30	4.68	4.02

semi-minor axis termed b. The derivation of the equations is rather involved and will not be given in detail here, but can be obtained from Gay (1968a).

The equations derived by Gay (Gay 1968a; equations 14 and 15), that describe the change in orientation of a particle $R(\theta, \phi)$ (see Fig. 8 for θ, ϕ definitions) due to a given coaxial plane strain, defined by the principal quadratic elongations of the strain ellipse λ_1, λ_2, to $R'(\theta', \phi)$ are:

$$\ln(\cot\phi') = \ln(\cot\phi) + [(a^2 - b^2)/(a^2 + b^2)] \ln[\sqrt{(\lambda_2/\lambda_1)}] \quad (11)$$

and

$$\cot\theta'/\cot\theta = \sqrt{(\sin 2\phi/\sin 2\phi')}, \quad (12)$$

which solves to

$$\theta' = a \tan\{\tan\theta[\sqrt{(\sin 2\phi/\sin 2\phi')}]\}. \quad (13)$$

The equation for ϕ' is not defined for azimuth angles of $\phi = 0$, 90, 180, 270, 360°. If ϕ is parallel to one of the principle coordinate axes, ϕ remains unchanged and only θ changes its value according to

$$\ln(\cot\theta') = \ln(\cot\theta) \pm 0.5[(a^2 - b^2)/(a^2 + b^2)] \ln[\sqrt{(\lambda_2/\lambda_1)}], \quad (14)$$

where the sign of the second part of the equation is positive, when ϕ is 0° or 180° and negative when ϕ is 90° or 270°.

Using these equations under the assumption that the principle susceptibility axes are parallel to the ellipsoid axes, as it was derived for magnetite grains (Uyeda *et al.* 1963), it is possible to simulate the strain response of the magnetic fabric.

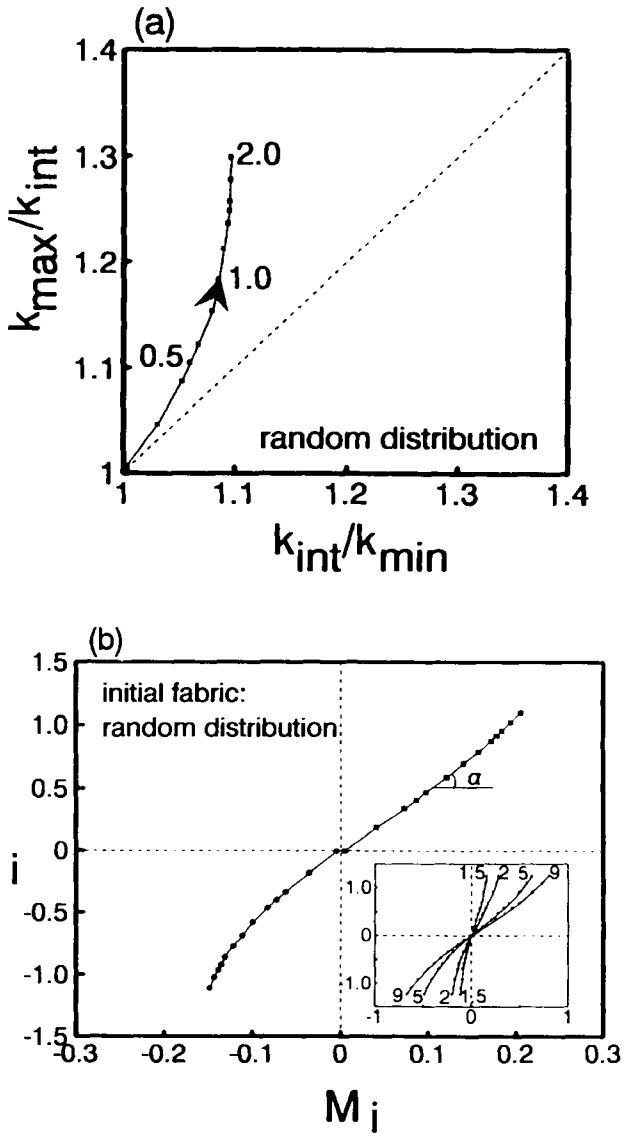

Figure 3. The strain response of the magnetic fabric of the initial randomly distributed grains during progressive March deformation under coaxial plane strain (compare fabric diagrams Fig. 2). (a) Flinn diagram (Flinn 1962), and (b) a correlation diagram between the natural strain ϵ_i and the magnetic parameter $M_i = \ln[k_i/(k_{max} \cdot k_{int} \cdot k_{min})^{1/3}]$. Squares correlate the maximum axes (positive values) and circles the minimum axes (negative values) separately. The correlation line of the maximum axes is log-linear for strain magnitudes up to 200 per cent; the minimum axes deviate from a log-linear correlation at strain magnitudes much lower than 200 per cent (prolate particles). Inset shows the dependence of the slope α on the particle anisotropy; numbers are values of k_{max}/k_{min}.

Results from the viscous fluid model

The viscous fluid strain response model was applied to deform the synthetic fabrics of an initial random distribution, and a girdle distribution in the xz-plane. The influences of coaxial plane strain on the resulting magnetic fabric were investigated in Flinn diagrams and magnetic fabric–strain magnitude correlation curves.

The application of this model is, in contrast to the March model, suited to simulate the behaviour of different shaped ellipsoids during deformation. The strain geometry, however, is restricted to plane strain deformations. To investigate the relationship between grain shape, strain, and magnetic fabric a multiparticle system with 300 randomly distributed grains (Fig. 9) was deformed at various strain magnitudes. Three different axial ratios $a:b = 2:1$, 5:1, and 10:1 were used for the simulations to study the effect of particle shape on the strain response of magnetic fabrics.

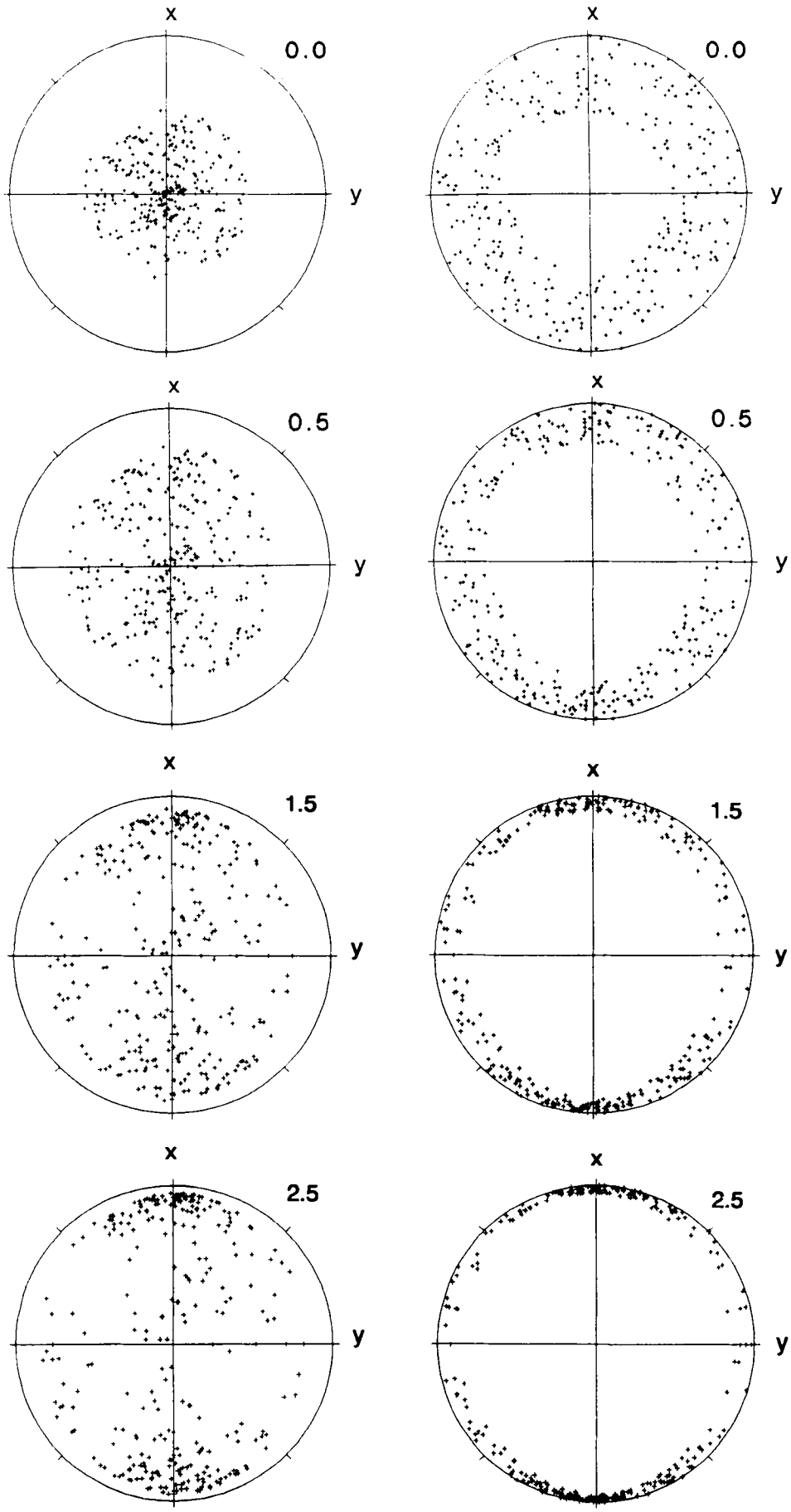

Figure 4. Fabric diagrams showing the behaviour of initial point (45° cone around z) and xy-girdle distributions during deformation with the March model. The numbers are the magnitudes of the elongation e_{11}; x is the extension direction.

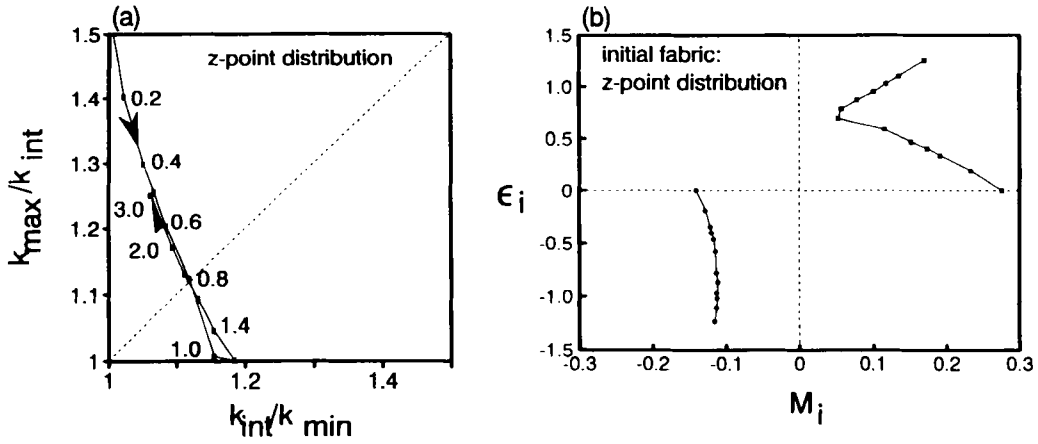

Figure 5. The magnetic fabric path of the point distribution (45° cone around z) during strain (a) in a Flinn diagram, and (b) in a strain versus magnetic fabric diagram. The ellipsoid shapes are ambiguous and can be correlated to different strain magnitudes. The minimum axes rotate approximately parallel to the y-axis with little change in their orientation. They reveal no correlation with the applied strain magnitude.

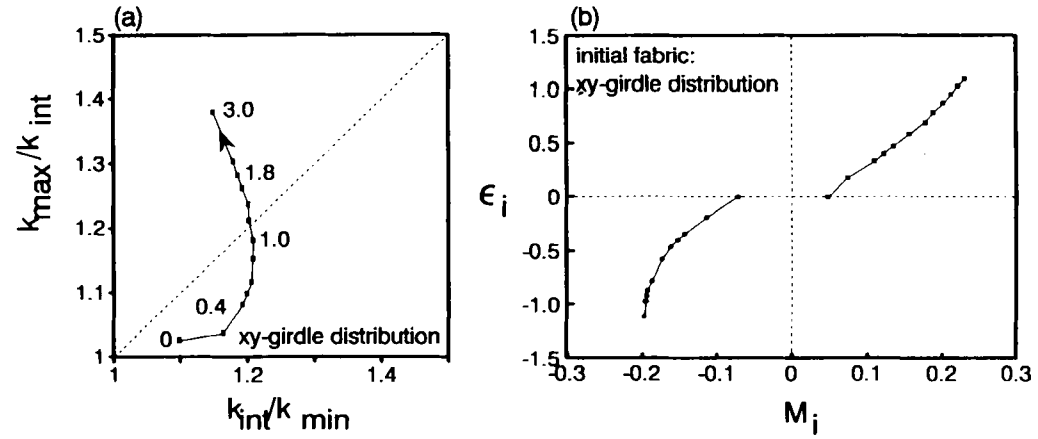

Figure 6. The magnetic fabric traced by the xy-girdle distribution during increasing strain (March model). (a) Flinn type diagram; numbers indicate the elongation e_{11}; and (b) strain versus magnetic fabric correlation diagram. The minor axes have an initial preferred orientation and do not noticeably rotate if the strain exceeds 60 per cent.

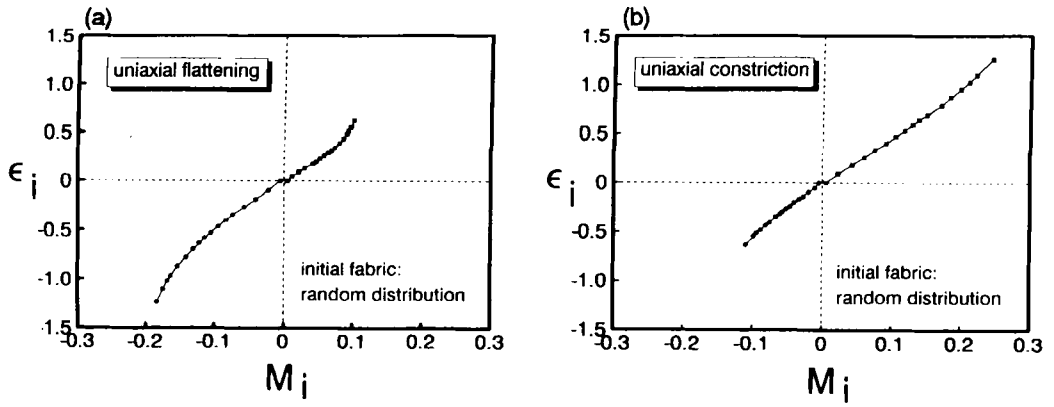

Figure 7. Strain versus magnetic fabric diagrams for equal-volume deformations with (a) uniaxial flattening, and (b) uniaxial constriction geometries calculated with the March model. Both diagrams show almost the same characteristics and are comparable with the results obtained by plane strain deformations.

Table 2. Principal strain magnitudes and susceptibilities for initial isotropic and *xz*-girdle distributions deformed after the March model and the Jeffery/Gay model under different strain geometries.

March model										Jeffery/Gay model							
flattening (e11=e22)					constriction (e22=e33)					random (e22=0)					xz-girdle (e22=0)		
e11	e33	k11	k22	k33	e11	e33	k11	k22	k33	e11	e33	k11	k22	k33	k11	k22	k33
0.00	0.00	5.03	5.00	4.98	0.0	0.00	5.03	5.00	4.98	0.0	0.00	5.03	5.00	4.98	5.11	5.38	4.11
0.05	-0.09	5.11	4.99	4.90	0.1	-0.05	5.12	4.95	4.94	0.1	-0.09	5.09	5.02	4.90	5.59	5.30	4.11
0.10	-0.17	5.20	4.97	4.82	0.2	-0.09	5.22	4.90	4.88	0.2	-0.17	5.13	5.01	4.86	5.70	5.19	4.11
0.14	-0.23	5.28	4.96	4.75	0.3	-0.13	5.31	4.86	4.83	0.3	-0.23	5.27	5.00	4.73	5.80	5.09	4.11
0.19	-0.29	5.37	4.94	4.69	0.4	-0.15	5.39	4.83	4.79	0.4	-0.29	5.35	4.99	4.66	5.89	5.00	4.11
0.22	-0.33	5.44	4.92	4.64	0.5	-0.18	5.47	4.79	4.74	0.5	-0.33	5.43	4.97	4.60	5.97	4.92	4.11
0.26	-0.37	5.50	4.91	4.59	0.6	-0.21	5.54	4.76	4.70	0.6	-0.37	5.49	4.96	4.55	6.05	4.83	4.11
0.30	-0.41	5.57	4.89	4.55	0.7	-0.23	5.61	4.73	4.66	0.7	-0.41	5.55	4.95	4.50	6.12	4.77	4.11
0.34	-0.44	5.62	4.87	4.51	0.8	-0.25	5.67	4.70	4.63	0.8	-0.44	5.61	4.94	4.46	6.18	4.71	4.11
0.37	-0.47	5.68	4.85	4.48	0.9	-0.27	5.72	4.68	4.60	0.9	-0.47	5.66	4.93	4.41	6.24	4.65	4.11
0.41	-0.50	5.72	4.83	4.45	1.0	-0.29	5.78	4.65	4.57	1.0	-0.50	5.70	4.92	4.38	6.29	4.60	4.11
0.47	-0.54	5.81	4.80	4.39	1.2	-0.33	5.89	4.60	4.51	1.2	-0.54	5.81	4.86	4.32	6.38	4.52	4.10
0.54	-0.58	5.89	4.76	4.35	1.4	-0.35	5.96	4.57	4.47	1.4	-0.58	5.88	4.84	4.27	6.46	4.45	4.10
0.62	-0.62	5.95	4.73	4.32	1.6	-0.38	6.04	4.53	4.43	1.6	-0.62	5.94	4.82	4.24	6.52	4.39	4.10
0.67	-0.64	6.01	4.70	4.29	1.8	-0.40	6.11	4.50	4.40	1.8	-0.64	5.99	4.80	4.21	6.57	4.34	4.09
0.74	-0.67	6.07	4.67	4.26	2.0	-0.42	6.16	4.47	4.36	2.0	-0.67	6.04	4.79	4.18	6.61	4.30	4.09
0.86	-0.71	6.17	4.61	4.22	2.5	-0.47	6.29	4.41	4.30	2.5	-0.71	6.13	4.79	4.13	6.70	4.22	4.08

Though P of shape anisotropic minerals is directly related to the grain shape (Uyeda *et al.* 1963), the magnetic properties of the particles were kept constant at $P = 1.75$ to study particle shape influences exclusively.

Five deformation steps of the multiparticle system containing grains with an axial ratio of $a:b = 5:1$ are shown in Fig. 9, the strain and anisotropy data together with the corresponding data of the *xz*-girdle are given in Table 2.

Comparing the particle distributions obtained from the March model (Fig. 2) with the results from the Jeffrey/Gay model (Fig. 9), a difference is not apparent. The establishment of preferred orientation takes, depending on the ellipsoid shape, a slightly different path. Consequently, the magnetic fabric reaches different final magnitudes. Fig. 10(a) shows the magnetic fabric path that was followed by the resultant principal magnitudes of all simulations, regardless of the various grain shape ratios. The isotropic initial magnetic fabric evolves to a prolate shape when the semi-major axes rotate into the extensional direction (compare Fig. 3a). Multiparticle systems containing grains with a higher axial ratio reach a better alignment of grain axes at the same strain magnitude. Hence, their development on the magnetic fabric path is more advanced compared to systems containing particles with lower axial ratios. The reason is the faster rotation of the long axes of rod-shaped particles than of nearly equidimensional particles. The stars on the curve (Fig. 10a) represent the final ellipsoid shapes reached after a strain of 250 per cent in the systems containing grains with various axial ratios.

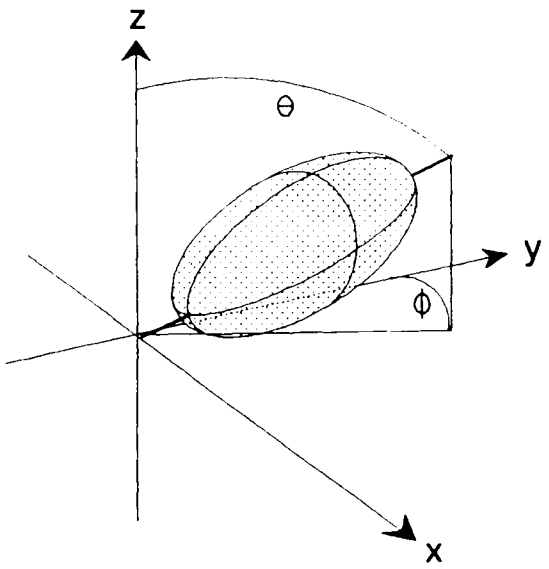

Figure 8. A prolate ellipsoidal particle in the Cartesian reference frame.

The relationship between M_i and the natural strain is shown in Fig. 10(b). A simple mathematical formulation for the curves is not apparent, but it is best approximated by a straight line. The correlation curves are similar in magnitude and shape to those calculated with the March model. Again the maximum axes behave in a linear fashion whereas the minimum values, especially of the rod-shaped particles, tend to deviate from the log–linear correlation when M_{min} approaches the maximum of -0.187 determined by the particle anisotropy. Fig. 10(b) also demonstrates that the slope of the curves is a function of the axial ratio of the grains. Elongate grains react faster to strain than spherical grains. Consequently, they are more perfectly aligned than the spherical ones, and the total multiparticle system reveals a stronger magnetic fabric for a given strain magnitude.

The deformation of the *xz*-girdle is shown in Fig. 11. The data are given in Table 2. The girdle was selected to cover a 40° area between two small circles. It disperses during progressive strain and the points rapidly commence clustering around the *x*-direction. The oblate initial fabric changes successively into a prolate magnetic fabric (shown in the Flinn-type diagram Fig. 12a). Only the long axes of the particles and, hence, the maximum susceptibility axes rotate in the *xz*-plane and move towards the extensional direction. The intermediate/minimum axes are nearly parallel to the *y*-direction and therefore hardly change their orientation. This behaviour is reflected in the strain–magnetic fabric correlation curves in Fig. 12(b). The maximum values reveal a nearly log–linear correlation. However, due to the high initial M_{max} the maximum possible magnetic parameter is rapidly reached and deflection from the linear correlation commences at 150 per cent strain. The magnitudes of the

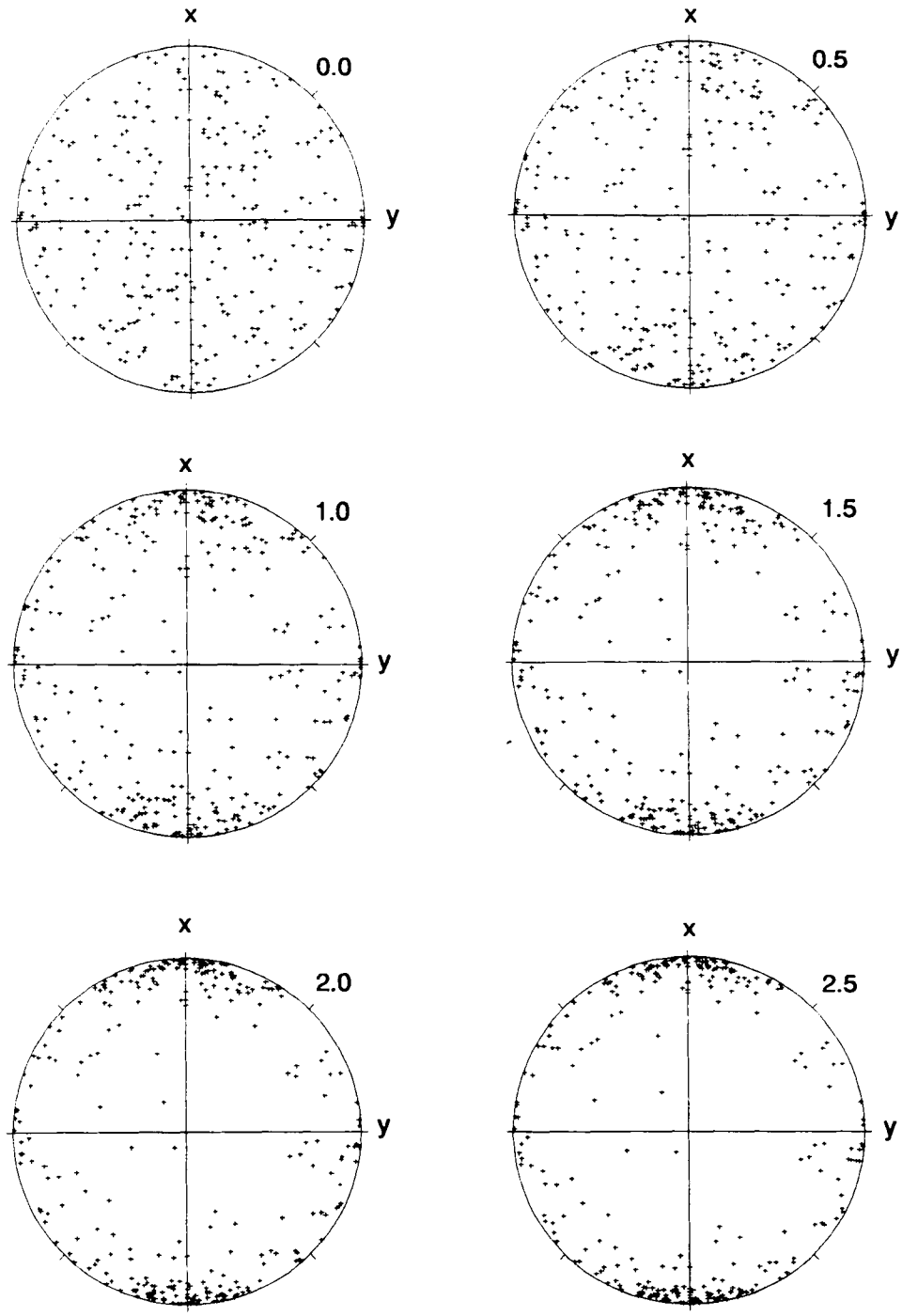

Figure 9. The distribution of 300 random points prior to the deformation with the Jeffrey/Gay model and five calculated deformation stages. The numbers are the magnitudes of the elongation e_{11}.

minimum axes are not a function of strain, because they do not change their orientation in the reference frame.

DISCUSSION

Numerical modelling was used to investigate the effects of initial grain distribution, single particle anisotropy, grain shape, strain magnitude and geometry, and the assumed strain-response model on the magnetic fabric of multiparticle systems. The simulations revealed a strong dependence of the final magnetic fabric on the distribution pattern of the initial fabric and on the single particle anisotropy. The effects of different strain geometries were investigated with the March model and appeared to be negligible for the correlation diagram. The comparison between the March and the Jeffrey/Gay model shows that the calculated grain orientations are quite similar in distribution and the magnitudes of the magnetic fabric of comparable order. Both models use ellipsoids of revolution as carriers of the

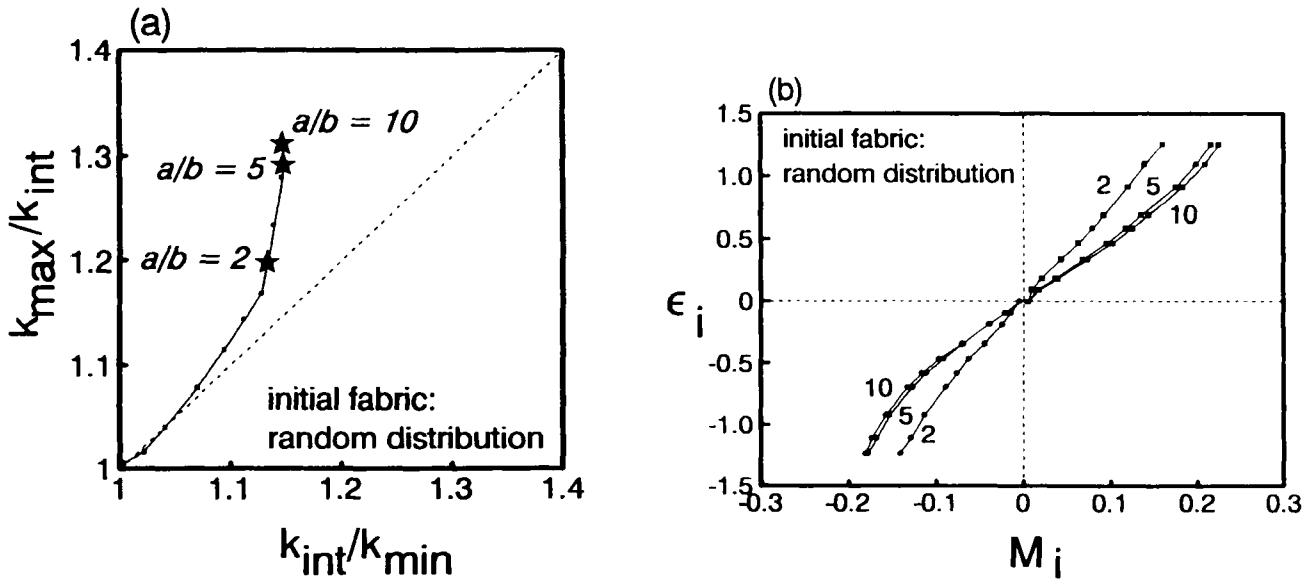

Figure 10. Magnetic fabric path of three different shape ellipsoids (a) in a Flinn type diagram. The final magnetic fabric after a strain of 250 per cent for the different ellipsoid forms is marked with a star. (b) M_i versus ϵ_i graph for the variously shaped ellipsoids. The numbers indicate the axial ratios a/b. for large ratios and grain rotation is faster than for small ratios and the magnetic fabric is more evolved.

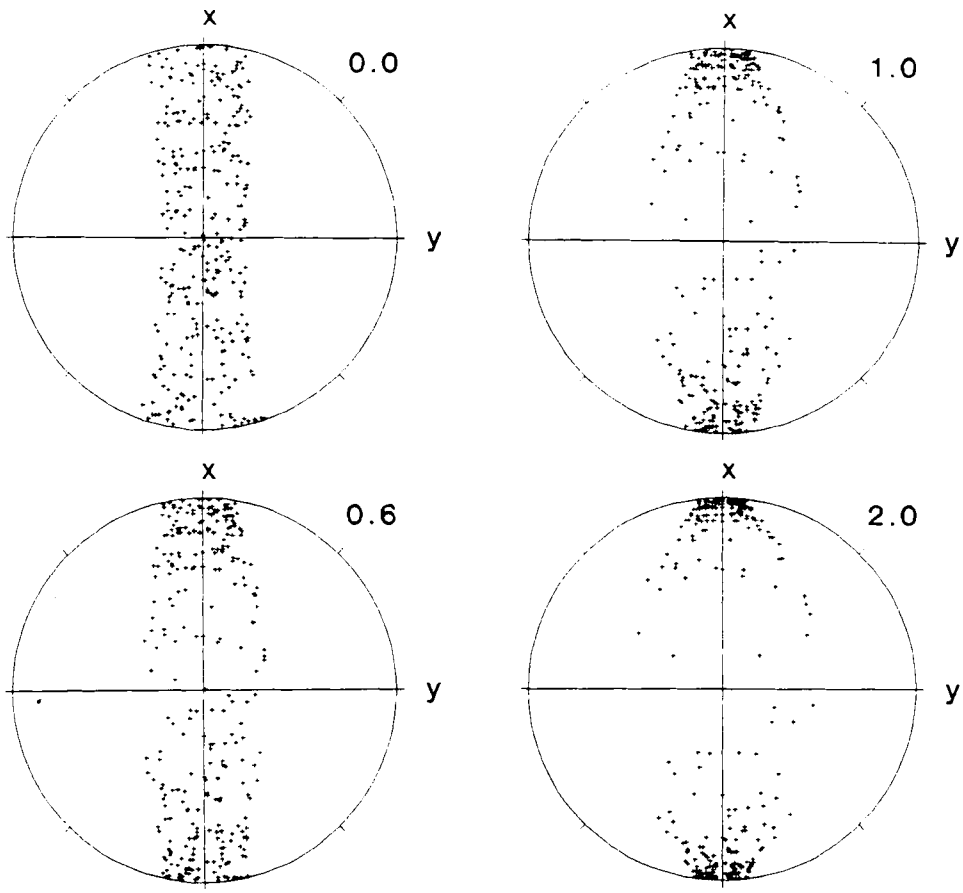

Figure 11. Fabric diagrams for the reorientation of an xz-girdle distribution with the viscous fluid model. Numbers are the magnitudes of elongation e_{11}.

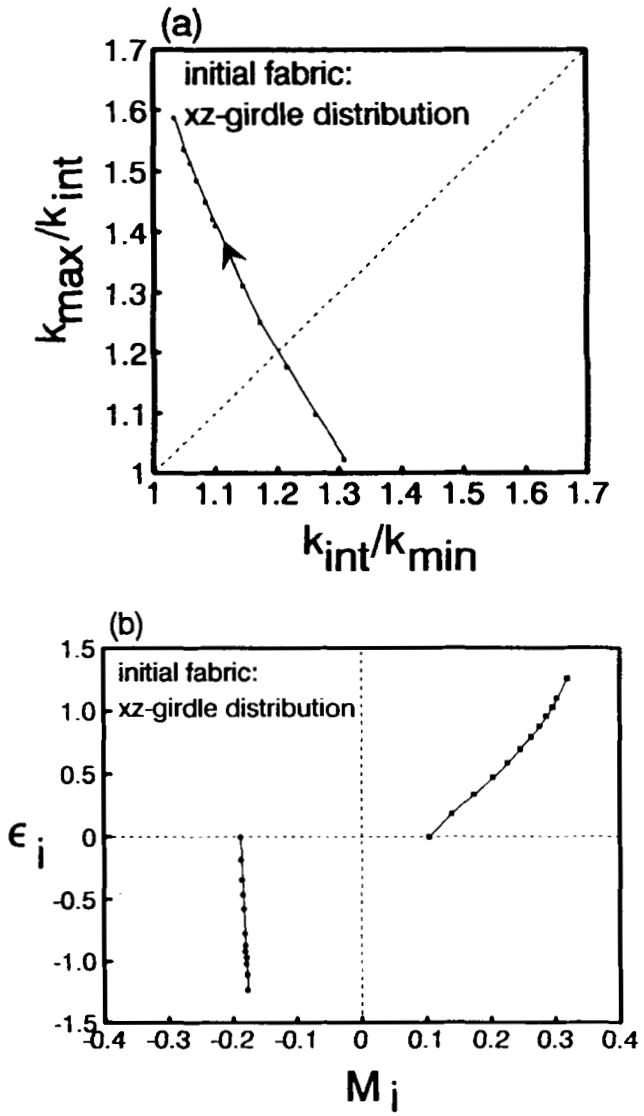

Figure 12. The magnetic fabric path followed by an initial xz-girdle distribution during coaxial strain calculated with the Jeffery/Gay model (a) in a Flinn type diagram, and (b) in a ϵ_i versus M_i diagram. Major axes reveal log-linear correlation, whereas the minor axes are unaffected by strain.

magnetic fabric. Hence, the intermediate and the minimum axes of a nearly perfectly aligned multiparticle system are equal and the maximum axis is longer, which results in a prolate magnetic fabric. The ellipsoid shapes for 0, 50, 100, and 200 per cent strain of the magnetic fabrics of all investigated systems are plotted together in a Flinn diagram in Fig. 13. The 200 per cent strained examples all (except the uniaxial flattened) have a prolate anisotropy, whereas lower strains produced partly oblate and partly prolate forms depending on the initial fabric. The shape of the magnetic fabric alone, hence, is not an indicator of the strain geometry or magnitude. The quantitative correlation between the magnitudes of the maximum natural strain and the magnetic parameter M_{max} yielded a nearly log-linear correlation for most initial distributions and strain geometries provided that the strain magnitudes are ≤200

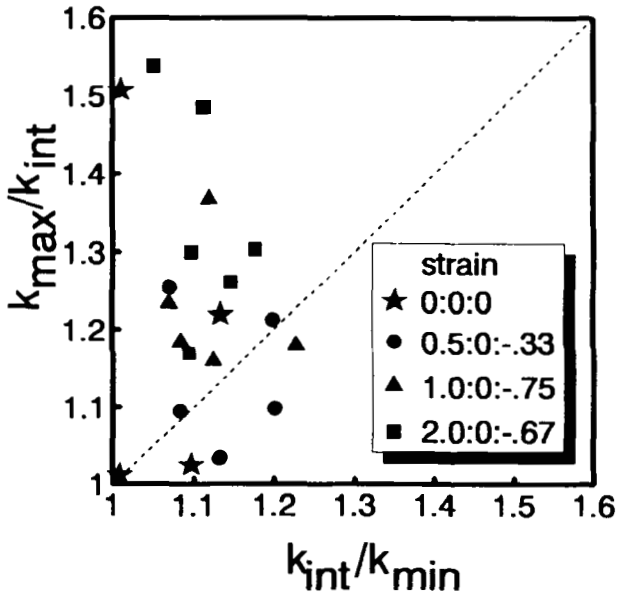

Figure 13. The results of all magnetic fabric–strain response models in a Flinn type diagram. With the exception of the particle mixture, all multiparticle systems were made up of particles with an anisotropy of 7:4:4.

per cent (Fig. 14). The slope $\alpha = \Delta\epsilon_i/\Delta M_i$ of the correlation curves (Fig. 14) decreases with increasing single grain anisotropy and with increasing ellipsoid ratio (Jeffery/Gay model). It is characteristic for a given mineralogy, initial grain distribution, and strain response and, hence, can be

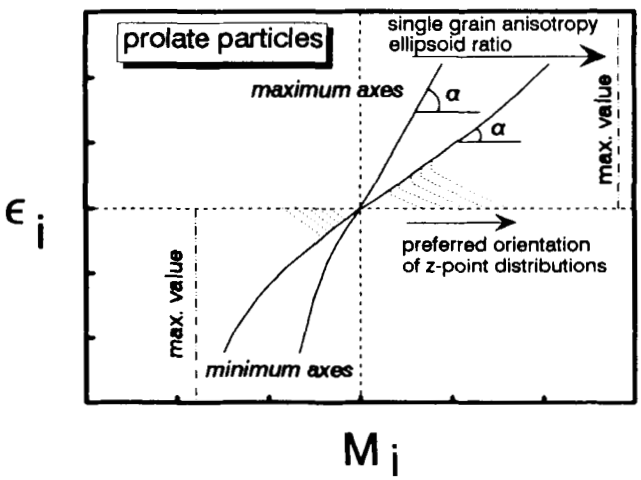

Figure 14. Schematic diagram of the magnetic fabric path of prolate particles for strains below 200 per cent. The slope of the linear segment of the correlation curves is a function of the anisotropy of the particles present and their shape, that influences the velocity of particles motion. Dashed lines represent initially anisotropic z-parallel clustering; the maximum values for the M_i parameter are determined by the particle anisotropy. For prolate particles the maximum M_i value of the minimum axes is lower than the corresponding value of the maximum axes. Therefore the maximum axes are log-linearly correlated to strain magnitudes up to 200 per cent, whereas the minimum axes deflect already at lower strain magnitudes from a linear correlation.

used for an estimation of strain, if all the variables are known and the assumptions of the models are fulfilled. If 200–300 per cent strain is exceeded, the M_i value starts to approach the maximum value defined by the single particle anisotropy asymptotically and the relationship is no longer log–linear. Point clusters and other preferred orientations lead to an initial M_i. The magnitudes of the initial M_i depend on the degree of the preferred orientation (compare Fig. 5b, 6b and 7b). The dashed lines in Fig. 14 symbolize this pattern for initial z-parallel clusters.

The minor axes in general show a different behaviour, because the limiting absolute values of M_{min} for prolate particles are lower than the limiting M_{max} values. This means that a divergence from the log–linear behaviour occurs at lower strains than for the maximum axes. An initial preferred orientation has a stronger influence on the M_{min} behaviour and often leads to non-correlation to the strain magnitudes. The major axes of the xz-girdle, for instances, correlate log–linear to strain, whereas the minor axes do not noticeably rotate (Fig. 12).

The final consequence from the model calculation for the quantitative correlation between the magnetic fabric and the strain in natural rocks is that a correlation exists with several configurations of the initial fabric, provided that the magnetic properties of the contributing minerals are known. For magnetite-dominated rocks, remanent anisotropies, or other one-mineral dominated anisotropies, the strain magnitude can be determined if modification of the magnetic fabric results from a passive rotation of the magnetic fabric carriers and these carriers can be characterized. Magnetite or ilmenite is likely not to recrystallize at lower temperatures and strain estimates were obtained from rocks that lack conventional strain markers using computer modelling of one-mineral dominated magnetic fabrics (Housen, Richter & von der Pluijm 1991).

CONCLUSIONS

The strain-response modelling of variously distributed multiparticle systems and the effect of initial fabric patterns and coaxial strain geometries and magnitudes on the final magnetic fabric demonstrates the following.

(1) The magnetic fabric path at different amounts of coaxial strain is a function of the orientation and distribution pattern of the initial fabric, the applied strain, and the strain-response model. The influences of the strain geometry are subordinate.

(2) A log–linear correlation between the natural strain ϵ_i and an associated magnetic parameter $M_i = \ln[k_i/(k_1 \cdot k_2 \cdot k_3)^{1/3}]$ exists for initially random distributions and strain magnitudes $\leq$200 per cent. The slope α of the correlation line is characteristic for the mineral composition of the magnetic phase.

(3) For strain magnitudes >200 per cent the M_i values asymptotically approach the single mineral M_i and the correlation is no longer log–linear.

(4) When initially anisotropic fabrics are strained, one of the principal magnetic axes correlates well with strain, whereas the others may not be affected. This is the consequence of preferred orientation and single particle anisotropy. For rocks containing prolate particles the maximum axis in general is a good strain indicator.

(5) One-mineral dominated magnetic fabrics can be used for a finite strain estimate, if the initial magnetic fabric is known, the magnetic carriers can be characterized and a passive rotation is demonstrated.

ACKNOWLEDGMENTS

This paper is based on parts of my PhD thesis at the University of Tübingen and completed during a post-doctoral stay at the University of Michigan. I would like to thank Wolfgang Frisch and Lothar Ratschbacher for their support, Jörg Braun for his valuable help during programming of the numerical models, and Dieter Krejci for the program of a high-quality outprint of the directional data. Reviews from Ben van der Pluijm, Bernie Housen, Joe Meert, and Susanne Borchert on earlier versions of the paper were most helpful. The many discussions with Ben led to a recalculation of the models and a reinterpretation of the results. Funding from the Land Baden-Württemberg and the Deutsche Forschungsgemeinschaft (DFG grant RI 567/1-1) is gratefully acknowledged.

REFERENCES

Bhattacharyya, D. S., 1966. Orientation of mineral lineation along the flow direction in rocks, *Tectonophysics*, **3**, 29–33.

Borradaile, G. J., 1987. Anisotropy of magnetic susceptibility: rock composition versus strain, *Tectonophysics*, **138**, 327–329.

Borradaile, G. J., 1988. Magnetic susceptibility, petrofabrics and strain—a review, *Tectonophysics*, **156**, 1–20.

Borradaile, G. J., 1991. Correlation of strain with anisotropy of magnetic susceptibility (AMS), *Pageoph.*, **135**, 15–29.

Borradaile, G. J. & Puumala, M. A., 1989. Synthetic magnetic fabrics in a plasticene medium, *Tectonophysics*, **164**, 73–78.

Borradaile, G. J., Keeler, W., Alford, C. & Sarvas, P., 1987. Anisotropy of magnetic susceptibility of some metamorphic minerals, *Phys. Earth planet. Inter.*, **48**, 161–166.

Bronstein, I. N. & Semendjaev, K. A., 1987. *Taschenbuch der Mathematik*, Harri Deutsch, Thun und Frankfurt/Main.

Cheeney, R. F., 1983. *Statistic Methods in Geology*, George Allen & Unwin, London.

Cogné, J. P., 1987. TRM deviations in anisotropic assemblages of multidomain magnetite, *Geophys. J. R. astr. Soc.*, **91**, 1013–1023.

Cogné, J. P. & Perroud, H., 1988. Anisotropy of magnetic susceptibility as a strain gauge in the Famanville granite, NW France, *Phys. Earth planet. Inter.*, **51**, 264–270.

Einstein, A., 1896. Eine neue Bestimmung der Moleküldimensionen, *Ann. d. Physik*, **19**, 289.

Ellwood, B. B., Hrouda, F. & Wagner, J.-J., 1988. Symposia on magnetic fabrics: introductory comments, *Phys. Earth planet. Inter.*, **51**, 249–252.

Flinn, D., 1962. On folding during three-dimensional progressive deformation, *Geol. Soc. Lond., Quart. J.*, **118**, 385–433.

Gay, N. C., 1966. Orientation of mineral lineation along the flow direction in rocks: a discussion, *Tectonophysics*, **3**, 559–564.

Gay, N. C., 1968. Pure shear and simple shear deformation of inhomogeneous viscous fluids. 1. Theory, *Tectonophysics*, **5**, 211–234.

Gay, N. C. 1968a. The motion of rigid particles embedded in a viscous fluid during pure shear deformation of the fluid, *Tectonophysics*, **5**, 81–88.

Henry, B. & Daly, L., 1983. From qualitative to quantitative

magnetic anisotropy analysis: The prospect of finite strain calibration, *Tectonophysics*, **98,** 327–336.

Hirt, A. M., 1986. Paleomagnetic and magnetic anisotropy techniques applied to tectonically deformed regions, *PhD thesis*, ETH Zürich.

Housen, B. A., Richter, C. & van der Pluijm, B. A., 1991. Finite strain modelling of magnetic anisotropy results from an anorthosite ductile shear zone, *EOS Trans. Am. geophys. Un.*, **72,** 98.

Hrouda, F., 1980. Magnetocyrstalline anisotropy of rocks and massive ores: a methematical model study and its fabric implications, *J. Struct. Geol.*, **2,** 459–462.

Hrouda, F., 1982. Magnetic anisotropy of rocks and it application in geology and geophysics, *Geophys. Surv.*, **5,** 37–82.

Hrouda, F., Siemes, H., Herres., N. & Hennig-Michaeli, C., 1985. The relationship between the magnetic anisotropy and the *c*-axis fabric in a massive hematite ore, *J. Geophys.*, **56,** 174–182.

Jeffery, G. B., 1923. The motion of ellipsoidal particles immersed in a viscous fluid, *Proc. R. Soc. London A*, **102,** 161–179.

March, A., 1932. Mathematische Theorie der Regelung nach der Korngestalt bei affiner Deformation, *Z. Krist.*, **81,** 285–297.

McCabe, C., Jackson, M. & Ellwood, B. B., 1985. Magnetic anisotropy in the Trenton limestone: results of a new technique, anisotropy of anhysteretic susceptibility, *Geophys. Res. Lett.*, **12,** 333–336.

Means, W. D., 1976. *Stress and Strain, Springer*, New York.

Nagata, T., 1961. *Rock Magnetism*, Maruzen, Tokyo.

Nye, J. F., 1985. *Physical Properties of Crystals*, Oxford University Press, Oxford.

Oertel, G., 1983. The relationship of strain and preferred orientation of phyllosilicate grains in rocks—a review, *Tectonophysics*, **100,** 413–447.

Oertel, G., 1983. The relationship of strain and preferred orientation of phyllosilicate grains in rocks—a review, *Tectonophysics*, **100,** 413–447.

Owens, W. H., 1973. Strain modification of angular density distributions, *Tectonophysics*, **16,** 249–261.

Owens, W. H., 1974. Mathematical model studies on factors affecting the magnetic anisotropy of deformed rocks, *Tectonophysics*, **24,** 115–131.

Ramberg, H., 1975. Particle paths, displacement and progressive strain applicable to rocks, *Tectonophysics*, **28,** 1–37.

Rathore, J. S., 1980. The magnetic fabrics of some slates from the Borrowdale volcanic group in the English Lake District and their correlations with strains, *Tectonophysics*, **67,** 207–220.

Reed, L. J. & Tryggvason, E., 1974. Preferred orientations of rigid particles in a viscous matrix deformed by pure shear and simple shear, *Tectonophysics*, **24,** 85–98.

Richter, C., 1991. Modelling fabric—strain relationships, *EOS*, **72,** 98.

Richter, C., Frisch, W., Ratschbacher, L. & Schwarz, H.-U., 1992. The magnetic fabrics of experimentally deformed artificial clay-water dispersions, *Tectonophysics*, **200,** 143–155.

Ruf, A. S., Naruk, S. J., Butler, R. F. & Calderone, G. J., 1988. Strain and magnetic fabric in the Santa Catalina and Pinaleno mountains metamorphic core complex mylonite zones, Arizona, *Tectonics*, **7,** 235–248.

Schultz-Krutisch, T. & Heller, F., 1985. Measurement of magnetic susceptibility in Buntsandstein deposits from Southern Germany, *J. Geophys.*, **57,** 51–58.

Uyeda, S., Fuller, M. D., Belshé, J. C. & Girdler, R. W., 1963. Anisotropy of magnetic susceptibility of rocks and minerals, *J. geophys. Res.*, **68,** 279–291.